





Gap solitons in nanoscale YIG magnonic crystals

Maria A. Morozova ^{*}, Oleg V. Matveev , Dmitry V. Romanenko , and Vera V. Balaeva
Saratov State University, Saratov 410012, Russia

Sergey A. Gusev  and Nikita S. Gusev
Institute for Physics of Microstructures, Russian Academy of Sciences, Nizhny Novgorod 603950, Russia

Sergey A. Nikitov
Saratov State University, Saratov 410012, Russia
and Kotelnikov Institute of Radioengineering and Electronics, Russian Academy of Sciences, Moscow 125009, Russia

 (Received 21 May 2024; revised 26 July 2024; accepted 20 August 2024; published 4 September 2024)

The main features of the nonlinear pulse propagated in iron-yttrium-garnet magnonic crystal with thickness 100 nm and a periodic system of grooves on the surface are studied. We have demonstrated the possibility of the formation of gap solitons at a frequency inside the band gap of the magnonic crystal when the input signal power is increased. A further increase in the duration and power of the input pulse leads to the formation a series of gap solitons with a duration of about 10 ns. We have discovered that the threshold power of the gap solitons' generation is determined by the magnitude of the magnetic field.

DOI: [10.1103/PhysRevB.110.104408](https://doi.org/10.1103/PhysRevB.110.104408)

I. INTRODUCTION

The most important parameters of modern semiconductor electronics, such as high processing speed, small element size, low power consumption, and low thermal radiation have fundamental physical limitations. The rapid development of information technologies (IT) dramatically increases the requirements for systems for generation, intelligent processing, and transmission of large amounts of data. This, in turn, places higher demands on the element base of IT systems. The need to improve the element base stimulates the search for fundamentally new approaches and methods of information processing. One of the alternative concepts to overcome these limitations lies in the field of magnonics, in which magnons rather than electrons are used as information carriers [1–3]. At the same time, the choice of an adequate transmission medium is a fundamental issue for creating functional devices and solving the problems. The most promising approach in this direction is based on the use of shortwave magnon excitations in nanoscale periodic magnetic structures [4–6].

From the point of view of microwave electronics requirements, the most commonly used materials for practical applications are films of ferrite garnet (in particular, iron yttrium garnet [$\text{Y}_3\text{Fe}_5\text{O}_{12}$, YIG]) of micron [7,8] and nanometer [3,9] thickness on nonmagnetic garnet [usually gadolinium-gallium ($\text{Gd}_3\text{Ga}_5\text{O}_{12}$, GGG) substrates]. The successful use of this material is due to extremely low microwave losses and weak magnetic anisotropy [8,10]. Modern technologies of magnetron sputtering and liquid-phase epitaxy allow one to grow YIG films with thickness from 5 nm [11,12].

The use of periodic inhomogeneities in ferromagnetic waveguiding structures leads to a significant change in the characteristics of propagating waves, additional resonance interactions, and the appearance of new physical effects. Such structures, called magnonic crystals (MCs), due to the formation of band gaps (BGs)—nontransmission bands in the spectrum of spin waves (SW), are functionally more flexible and have more possibilities for controlling the spin-wave characteristics [8,13]. To date, the possibility of controlling the band gaps by means of electric and magnetic fields in MCs based on micron-thick YIG films, including a periodic system of grooves [14–16], a system of semiconductor [17] and ferroelectric [18,19] strips on the surface, and films with periodically changing width [20,21], has been demonstrated. MCs based on nanometer-thick films are also currently under active investigation [22–24]. Low losses in YIG films lead to the fact that, at relatively low levels of input power (about 1 μW), nonlinear effects of self-interaction are manifested during the propagation of spin waves in micron-thick YIG films. The main role in nonlinear processes in ferromagnetics is played by the increase in the precession angle of magnetic moments of atoms with increasing signal power, which leads to a change in the longitudinal component of the magnetic moment. As is known, the ferromagnetic medium is a medium with the Kerr type of cubic nonlinearity [25,26]. In recent years, there has been a growing interest of researchers in nonlinear effects in the propagation of spin waves, due to the active search for new approaches for the realization of neuromorphic computing [27–29]. In particular, nonlinearity is a prerequisite for a reservoir-based neuromorphic architecture, in which nonlinear mapping of low-dimensional sequential input data into higher-dimensional spatiotemporal data is realized in a physical reservoir based on a magnetic film and a feedback loop [29].

^{*}Contact author: mamorozovama@yandex.ru

Nonlinear phenomena in periodic ferromagnetic structures have so far been considered only for micron-thick films [30–33] and for nanometer-thick films [34]. To date, three-magnon parametric interactions in MCs [8,30] and four-magnon processes in such systems [31–33] have been studied. The main nonlinear effect in the field of four-magnon processes is the nonlinear shift of the band gaps by 5–15 MHz to the low-frequency region when the input signal power increases up to 80 mW [15]. As shown in that work, the transmission coefficient at the frequency of the band gap grows with increasing input signal power, which leads to the effect of “nonlinear MC switching,” in which the periodic structure begins to transmit a high-power signal at frequencies lying inside the band gap. By employing the nonlinear effects in YIG on dielectric substrates (GGG), the variety of tunable spin-wave devices was realized, e.g., intensity-dependent nonlinear phase shifters, filters, switching devices, etc. [32,35,36].

Another nonlinear phenomenon is the formation of envelope solitons—gap solitons (GSs) [31,33,37]. The concept of gap solitons was first introduced when describing pulses that are formed at the frequency of the input signal lying in the BG of a periodic structure. The GS is a certain combination of direct and reflected from periodic inhomogeneities’ waves, which are combined in such a way that they move together with reduced velocity [38]. One of the main properties of such GSs is that their velocity is smaller than the wave group velocity in a nonperiodic structure [39,40]. Nonlinear effects, in particular, the formation of envelope solitons, have so far been studied in ferrite nonperiodic structures [37,38]. The observation of GSs in periodic structures has been reported only for thick 10- to 15- μm -thick YIG films. In particular, in Ref. [37], gap solitons were experimentally observed in a 10- μm -thick YIG film with a periodic system of grooves on the surface at an input power of about 16 dBm. It should be expected that the formation of gap solitons is also possible in a nanometer-thick YIG film at lower input powers.

In the present work, we consider nonlinear phenomena in a 100-nm-thick YIG film with a periodic system of grooves on the surface. The possibility of the formation of nanosecond-long GSs, nonlinear switching, and nonlinear shift of the BG during the propagation of nonlinear spin waves has been investigated. The characteristics of the GSs depending on the amplitude and duration of the input pulse are revealed, as well as the possibility of controlling the GSs with the help of an external magnetic field.

The paper is structured in follows. Section II contains the experimental results for nonlinear spin waves propagating in a MC based on YIG film with a periodic system of grooves on the surface. Section III describes the theoretical model. The model was built using the method of coupled waves. Section IV contains the calculating results and discussions. Section V concludes the work.

II. EXPERIMENTAL INVESTIGATION

Figure 1(a) shows the layout of the investigated structure. The experimental layout was made on the base of YIG film with a thickness of $a = 100$ nm and a saturation magnetization of $4\pi M_0 = 1750$ G grown on the GGG substrate. On the surface of the YIG film with the ferromagnetic resonance

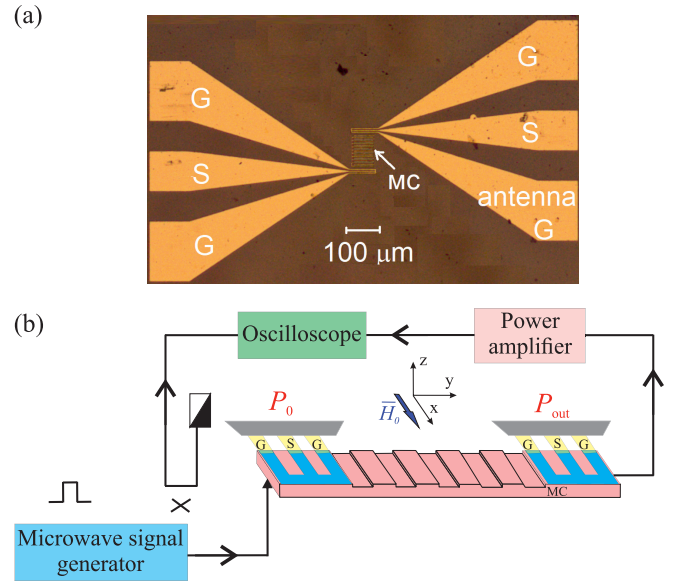


FIG. 1. (a) Secondary electron micrographs of the experimental layout. (b) The scheme of the experimental setup.

line-width 0.3 Oe, the periodic structure was created with the period $L = 4$ μm in the form of grooves with the depth $\Delta = 10$ nm and the width $b = 2$ μm . The length of MC $l = 80$ μm , and the width is $w = 50$ μm . To excite spin waves, coplanar ground-signal-ground (GSG) antennas (Au) with 2.4- μm stripe width and 2.5- μm stripe spacing were placed. The excitation and reception of spin waves was carried out due to coplanar GSG antennas (Au) deposited on the surface of the YIG film by optical lithography. The width of the strips was 2.5 μm , and the distance between the signal conductor and the grounding contacts was 2 μm . Microphotographs of the layout obtained in the electron microscope are shown in Fig. 1(a). The experimental setup included the layout of a transmission line based on MC, a microwave analyzer ENA 5062A circuits, a four-channel real-time oscilloscope Agilent DSO81004B, a microwave signal generator Agilent ESG E4438, and a low-noise power amplifier MAHW010120-01 [Fig. 1(b)]. An amplified signal from the output of the transmission line was applied to one of the channels of the oscilloscope, and a branched microwave signal from the generator was applied to the other. Microwave probes the Form Factor PC-GSG-150 mounted on precision positioners were used to connect the layout with signal sources and receivers. The external magnetic field was created by a quadrupole electromagnet. An external constant magnetic field H_0 was applied in parallel to the coplanar antennas, and surface spin waves were excited in the MC.

Figures 2(a) and 2(b) show the amplitude-frequency characteristics and the corresponding dispersion characteristics obtained from the phase-frequency characteristics of the spin waves at different input signal powers and a magnetic field magnitude of 560 Oe. It can be seen from Fig. 2(a) that, at $P_0 = -30$ dBm (green curve), a pronounced minimum is observed at the frequency $f_B^l = 4.459$ GHz, marked by gray fill. At the frequency f_B^l , a jump in the dispersion characteristic is also observed [Fig. 2(b)], with the wave number coinciding

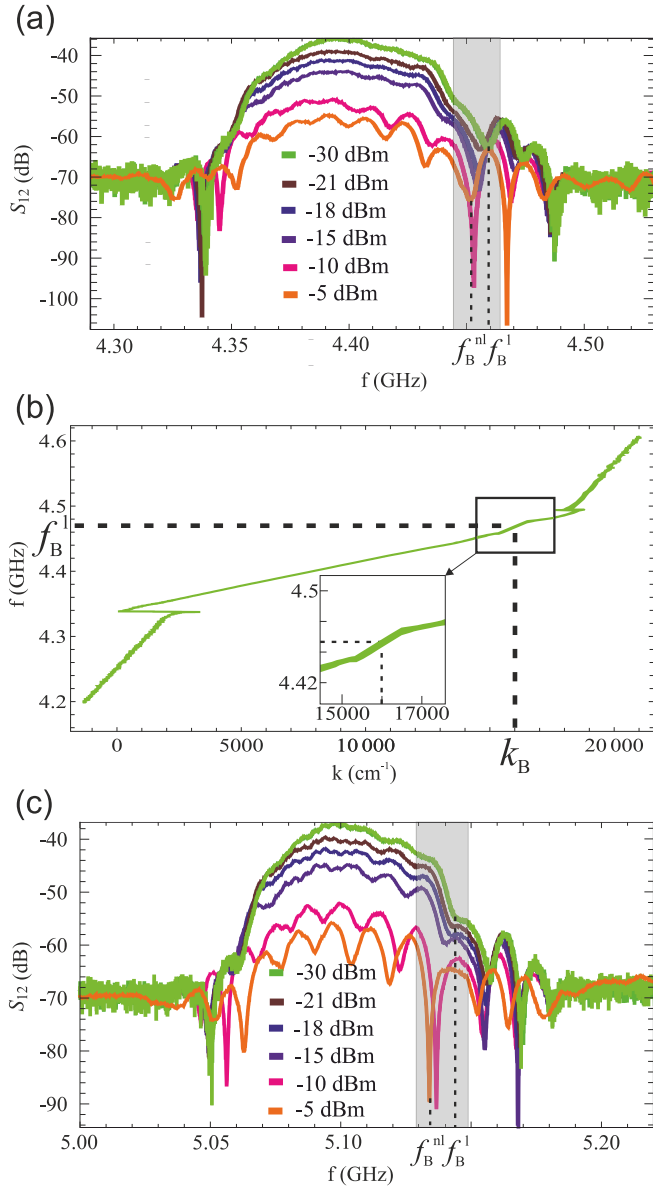


FIG. 2. The MSSW transmission in the MC and different input power P_0 at (a) $H_0 = 560$ Oe and (c) $H_0 = 780$ Oe. The S_{21} parameter was obtained with a vector network analyzer. The gray shading shows the band-gap regions. Symbols f_B^l and f_B^{nl} denote the center frequencies of the band gaps in the linear and nonlinear cases, respectively. (b) Dispersion characteristics at input power $P_0 = -30$ dBm and $H_0 = 560$ Oe. The inset shows an enlarged fragment of the dispersion characteristics in the BG region. The symbol k_B denotes the wave number corresponding to the center of the BG.

with the wave number of the second Bragg resonance $k_B = 2\pi/L = 15708$ $1/\text{cm}$. In the vicinity of f_B^l , a BG is formed, i.e., a band of nontransmittance of spin waves. When the input power is increased up to -5 dBm [orange curve in Fig. 2(a)], there is a nonlinear shift of the BG down the frequency by the order of 6 MHz and it is observed at $f_B^{nl} = 4.453$ GHz. This effect has been observed previously for 10- μm -thick MCs [15,37,41]. Figure 2(c) shows the amplitude-frequency characteristics of the spin waves at different input signal powers

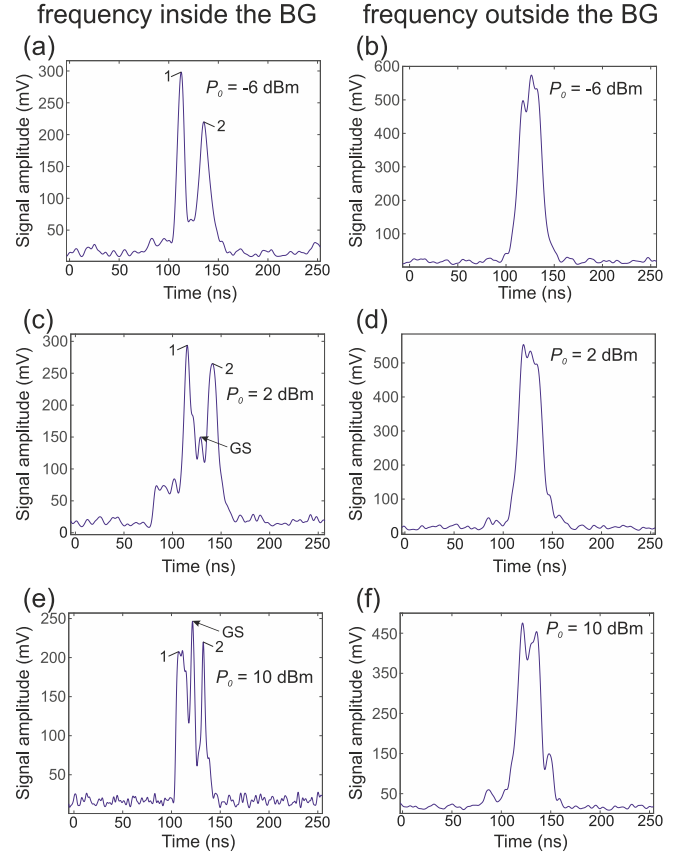


FIG. 3. Time profiles of output pulses at $H_0 = 560$ Oe, input pulse duration $\tau = 50$ ns, and different levels of pulse: (a), (b) $P_0 = -6$ dBm, (c), (d) $P_0 = 2$ dBm, and (e), (f) $P_0 = 10$ dBm. The left column shows profiles of output pulses with frequency inside the band gap $f = 4.459$ GHz, and the right column shows profiles of output pulses with frequency outside the band gap $f = 4.383$ GHz. Label “1” is the splash corresponding to the leading edge, label “2” is the splash corresponding to the trailing edge, and label “GS” is the gap soliton.

and a magnetic field magnitude of 780 Oe. It can be seen that the nonlinear shift down the frequency is 3 MHz.

At the next stage we consider the features of pulse signals passing through the investigated structure at different input signal powers P_0 . For this purpose, rectangular microwave pulses of 50- to 300-ns duration, 1- to 2- μs repetition rate, and carrier frequency lying inside the BG as well as outside the BG were fed to the input of the transmission line.

Let us first consider the passing of a rectangular microwave pulse with 50-ns duration through the MC and a magnetic field magnitude of 560 Oe. Figure 3 shows the envelope amplitude of the output pulse with the carrier frequency lying outside the BG $f = 4.383$ GHz (Fig. 3, right column) and inside the band gap $f = f_B^l = 4.459$ GHz (Fig. 3, left column). It can be seen that, at the frequency outside the BG, the shape of output pulse close to the shape of the input pulse. When the input power is increased, the pulse shape changes insignificantly. At the frequency inside the BG, the shape of the output pulse differs from that of the input pulse.

In the vicinity of frequencies near the BG, the amplitude frequency characteristic (AFC) of the transmission line is

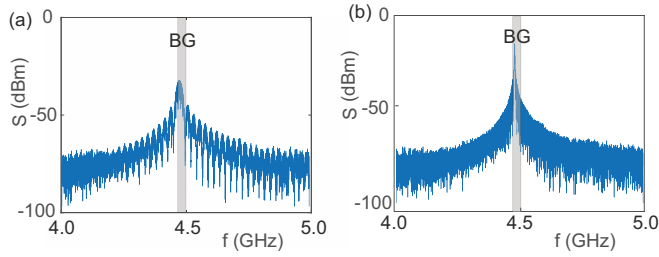


FIG. 4. Spectral characteristics of the input pulses with a duration of (a) 50 ns and (b) 300 ns. The BG area is marked with a gray fill. ($H_0 = 560$ Oe, $P_0 = -10$ dBm).

equivalent to the AFC of a notch microwave filter. Figure 4 shows the spectral characteristics of input pulses. The frequency area corresponding to the BG is marked with a gray fill. It can be seen that a large part of the pulse spectrum is located below the lower boundary of the BG. When a microwave signal with a finite width of the frequency spectrum, for example, a rectangular microwave pulse, is passing through the MC, its spectral components lying inside the band gap will be removed (significantly attenuated). In this case the carrier frequency $f = f_B^l$ will be removed and in the frequency domain there will be a splitting of the original signal spectrum into two regions lying above and below the center frequency of the BG. In this case the shape of the output envelope will be determined by the rate of amplitude change at the leading and trailing edges of the input pulse [42]. For time intervals where the envelope amplitude of the input signal is constant, the output signal will be zero. In the linear mode, only two splashes are observed in the output signal, corresponding to the leading and trailing edges of the input rectangular microwave pulse [Fig. 3(a)]. The interval between them is equal to the duration of the input pulse. These splashes are observed at any value of P_0 (marked by the arrows 1 and 2 in Fig. 3, left column).

As the input power increases to $P_0 = 2$ dBm, an additional pulse is formed in the output signal, which is not related to either the trailing or the leading edge of the input pulse. The occurrence of the additional pulse can be explained by the influence of the nonlinear precession of the magnetization vector in the MC, which is determined by the instantaneous power of the spin wave. This leads to the BG shift and the appearance of gap solitons. The physical mechanism of soliton formation is the mutual compensation of dispersion and nonlinearity [43]. The dispersion grows as we approach the center of the BG. If the pulse frequency coincides with the BG center frequency, dispersion prevails over nonlinearity and the input pulse becomes broadened. When the input power increases, the BG shifts and the carrier frequency of the pulse falls on the right slope of the BG, while the nonlinearity compensates the dispersion, which is necessary for soliton formation. The duration of the gap soliton is of the order of 10 ns. The amplitude of the gap soliton also increases with increasing input power. Previously, gap solitons were observed experimentally in optics for nonlinear Bragg gratings [38,43] and for 10- μm -thick MCs [37,41]. Figure 5 shows the spectra of output pulses at frequency inside and outside the BG at different input pulse power. It can be seen that at frequency inside the BG the amplitude of higher harmonics increases

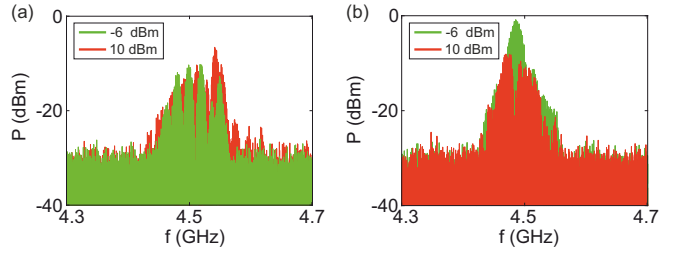


FIG. 5. Spectral characteristics of the output pulses with a duration of 50 ns at input power $P_0 = -6$ dBm (green curve) and $P_0 = 10$ dBm (red curve) at (a) frequency inside the BG $f = 4.459$ GHz and (b) frequency outside the BG $f = 4.383$ GHz.

with the increasing input pulse amplitude that is related to the BG shift.

Figure 6 (left column) shows the envelope amplitude of the output pulse for the input pulse with a duration of 100 ns at the frequency inside the BG $f = f_B^l = 4.459$ GHz. It can be seen that, at the input power $P = -16$ dBm, the formation of the GS is observed. Thus, the threshold power for the GS formation decreases compared to the case of 50-ns pulse duration. When the input signal power increases up to 6 dBm, the number of GSs increases, and their amplitude, width, and position on the time axis change (i.e., their speed).

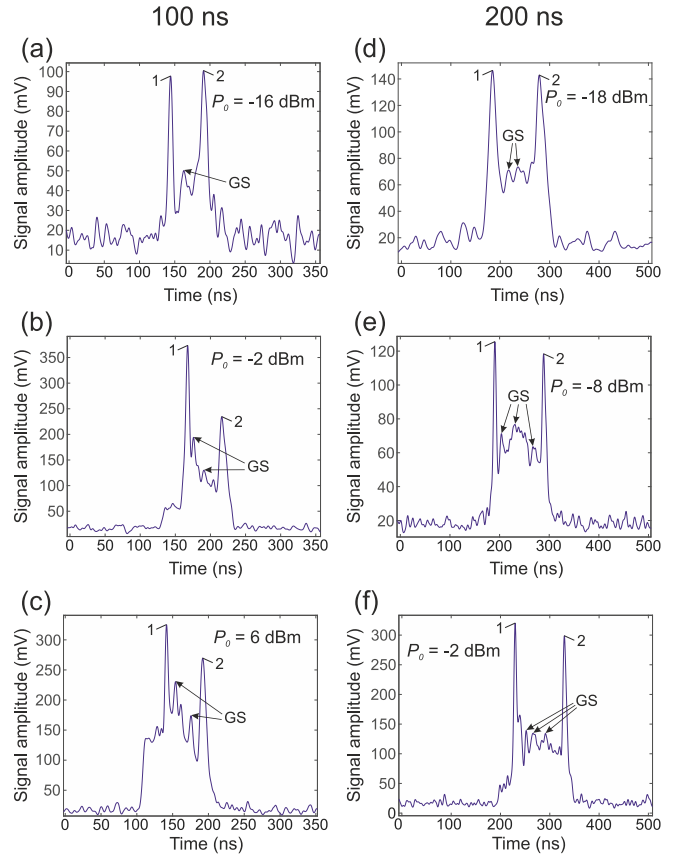


FIG. 6. Time profiles of output pulses with the frequency inside the band gap $f = 4.459$ GHz at $H_0 = 560$ Oe and input pulse durations of $\tau = 100$ ns (left column) and $\tau = 200$ ns (right column) and different levels of pulse P_0 .

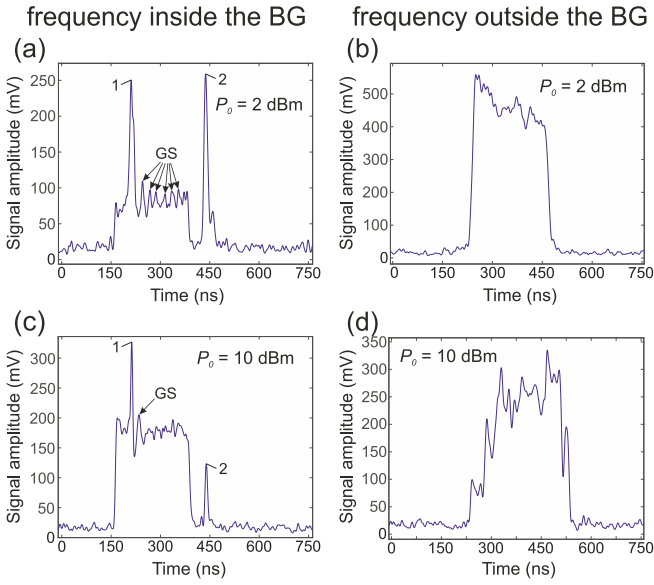


FIG. 7. Time profiles of output pulses at $H_0 = 560$ Oe and input pulse duration $\tau = 300$ ns and different levels of pulse: (a), (b) $P_0 = 2$ dBm and (c), (d) $P_0 = 10$ dBm. The left column shows profiles of output pulses with the frequency inside the band gap $f = 4.459$ GHz, and the right column shows profiles of output pulses with the frequency outside the band gap $f = 4.383$ GHz.

Figure 6 (right column) shows the envelope amplitude of the output pulse for the input pulse with a duration of 200 ns at the frequency inside the BG. It can be seen that the formation of the GS is observed at a lower input signal power of -18 dBm in comparison with the previous cases.

Figure 7 shows the envelope amplitude of the output pulse for the input pulse with a duration of 300 ns. It can be seen that the input signal with the frequency outside the BG with increasing input power leads to the insignificant change of the output pulse shape (Fig. 7, right column). When the input signal with the frequency lies inside the BG and the input power is 2 dBm, in contrast to the pulse duration of 50 ns [Fig. 3(c)], a sequence of pulses is formed, not one pulse. When the power is increased up to 10 dBm, the shape of the output pulse is close to the shape of the input pulse; i.e., the input pulse passes through the structure with insignificant distortions. This feature indicates a nonlinear shift of the BG and the carrier frequency a falling of the carrier frequency into the region lying outside the BG in the nonlinear case [Fig. 2(a)].

Figure 8 shows the envelope amplitude of the output pulse for the input pulse with a duration of 200 ns and another magnitude of the external magnetic field of 870 Oe. It can be seen that, at this magnitude of the magnetic field and an input signal power of -8 dBm, the GSs are not formed [Fig. 8(a)], in contrast to the magnitude of 560 Oe [Fig. 6(e)]. This feature is related to the fact that at this magnitude of the magnetic field the nonlinear shift of the BG is smaller and the frequency of the BG [see Fig. 2(c)]. Consequently, the GS formation threshold at this magnitude of the magnetic field is higher than that in the case of the 560-Oe field. When the power is increased to -2 dBm, the formation of a series of GSs is observed. At the

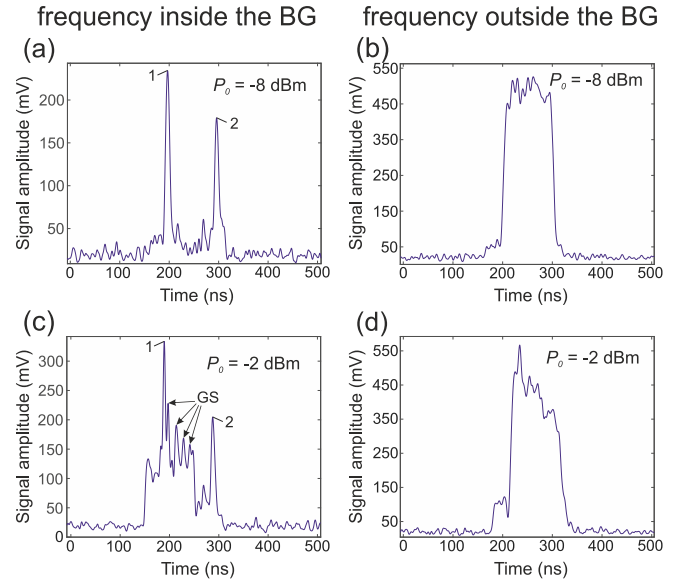


FIG. 8. Time profiles of output pulses at $H_0 = 870$ Oe and input pulse duration $\tau = 200$ ns and different levels of pulse: (a), (b) $P_0 = -8$ dBm and (c), (d) $P_0 = -2$ dBm. The left column shows profiles of output pulses with the frequency inside the band gap $f = 5.155$ GHz, and the right column shows profiles of output pulses with the frequency outside the band gap $f = 5.096$ GHz.

frequency outside the BG (Fig. 7, right column), the shape of the output pulse replicates the shape of the input signal and changes insignificantly.

III. THEORETICAL MODEL

To develop the theoretical model, we use the dispersion equation for spin waves in a ferromagnetic film without parameter modulation [39,40]. We apply the procedure of wave equation reconstruction from the dispersion equation. We introduce the following substitutions $\omega \rightarrow i\frac{\partial}{\partial t}$ and $k \rightarrow -i\frac{\partial}{\partial y}$, and at small kd for an infinite width film, we obtain the equation of magnetization vector motion in a ferromagnetic film in the following form:

$$\frac{\partial^2 m}{\partial t^2} = -\omega_{\perp}^2 m \pm \frac{\omega_M^2 d}{2} \frac{\partial m}{\partial y} - \gamma \frac{2A_{ex}}{M} \frac{\partial^2 m}{\partial y^2} + 2\alpha_0(\omega_H + i\alpha_0\omega) \frac{\partial m}{\partial t}, \quad (1)$$

where the “ $-$ ” sign refers to the wave propagating in the positive y direction, the “ $+$ ” sign refers to the wave propagating in the negative y direction, $m = m_x/M_0$ is the normalized high-frequency component of magnetization, $\omega_{\perp}^2 = (\omega_H + i\alpha_0\omega)(\omega_H + i\alpha_0\omega + \omega_M)$, $\omega_M = 4\pi\gamma M$ (in the linear case a longitudinal component of magnetic moments $M = M_0$), A_{ex} is the exchange constant, γ is the gyromagnetic ratio, H_0 is the external magnetic field, d is the ferromagnetic film thickness, $\alpha_0 = \frac{\Delta H}{H}$ is the parameter of dissipation, and ΔH is the width of the ferromagnetic resonance curve.

Nonlinear processes in ferromagnetics are caused by the decrease of the effective saturation magnetization with the increase of the amplitude of magnetization dynam-

ics. Thus, taking into account Kerr-type nonlinearity, the longitudinal components of magnetic moments can be presented as [25,26,44]:

$$M \approx M_0(1 - q|m|^2), \quad (2)$$

where $q = \frac{1}{2}(1 + \frac{\omega_H^2}{\omega_\perp^2})$ is the parameter of nonlinearity.

At the next stage, we take into account that a periodic system of grooves is placed on the surface of the ferromagnetic film. If the ferromagnetic film has the variable thickness, the value d in Eq. (1) is the periodic function that depends on the longitudinal coordinate y and has the following form [17,45]: $d = d_0 + \delta \cos(\pi y/L)$, where $d_0 = a - \Delta + \Delta b/L$, $\delta = \frac{2\Delta}{\pi d_0} \sin(\pi b/L)$, L is the period, Δ and b are the depth and the width of grooves, and a is the height of stacks. Thus, Eq. (1) has periodically varying coefficients. To solve this equation (for $\Delta \ll d_0$), an approach based on the method of coupled waves is used, which consists of the fact that waves propagating in the forward and backward directions (wave reflected from spatial inhomogeneities) in a periodic system are considered independently, and the periodic structure provides their coupling [46].

The solution of wave equation (1) with Eq. (2) can be presented as a sum of spatial harmonics [46]: $m = \sum_{n=-\infty}^{\infty} A_n \exp[ik_n y]$, where A_n are complex amplitudes of harmonics, and k_n are propagation constants. In the first Brillouin zone $0 \leq k_n L \leq 2\pi$, $n = \dots -2, -1, 0, 1, 2 \dots$, only zero harmonics of direct waves ($n = 0$) and “-1” wave harmonics of the waves reflected from spatial inhomogeneities ($n = -1$) are taken into account. In this case, the solution of wave equation (1) can be presented as the sum of direct and reflected waves:

$$m = A \exp[i(\omega t - k_0 y)] + B \exp[i(\omega t + k_{-1} y)], \quad (3)$$

where A and B are slowly changing complex amplitudes of envelopes of direct and reflected waves, k_0 is the propagation constant of zero harmonic, k_{-1} refers to “-1” harmonic, and $\omega = 2\pi f$ is the frequency of input signal (carrier frequency). Propagation constants k_0 and k_{-1} are connected by the Bragg condition: $k_{-1} = -k_0 + 2\pi/L$.

Substituting Eqs. (2) and (3) into Eq. (1) and considering $\frac{\partial^2 A}{\partial t^2} \ll \omega \frac{\partial A}{\partial t}$, $\frac{\partial^2 B}{\partial t^2} \ll \omega \frac{\partial B}{\partial t}$, $\frac{\partial^2 A}{\partial y^2} \ll \omega \frac{\partial A}{\partial y}$, and $\frac{\partial^2 B}{\partial y^2} \ll \omega \frac{\partial B}{\partial y}$, we obtain the following equations:

$$\begin{aligned} i \left(\frac{\partial A}{\partial t} + V \frac{\partial A}{\partial y} \right) + \eta_0 A + \kappa_0 B + \gamma_0 (|A|^2 + 2|B|^2) A + i\alpha A &= 0, \\ i \left(\frac{\partial B}{\partial t} - V \frac{\partial B}{\partial y} \right) + \eta_{-1} B + \kappa_{-1} A + \gamma_{-1} (|B|^2 + 2|A|^2) B - i\alpha B &= 0, \end{aligned} \quad (4)$$

where $V = \omega_M^2 d_0 / 2\omega$ is the group velocity, $\kappa_{0,-1} = \delta V k_{0,-1} / 2$ is the periodicity coefficient, $\gamma_{0,-1} = -q \frac{\omega_H \omega_M + 8\omega_M^2 d_0 k_{0,-1}}{4\omega}$ is the nonlinearity coefficient, $\eta_{0,-1} = \frac{\omega_\perp^2 - \omega^2 + \omega_M^2 d_0 k_{0,-1}}{2\omega}$ is the frequency detuning, $\alpha = \frac{\alpha_0 \omega_H}{2\omega}$ is the dissipation coefficient, and $\omega_H = \gamma H_0 + i\alpha_0 \omega - \gamma \frac{2A_{ex}}{M} k_{0,-1}^2$ is the ferromagnetic resonance frequency. Equation (4) is a nonlinear coupled-wave equation and describes the dynamics of the spin-wave envelopes in the MC.

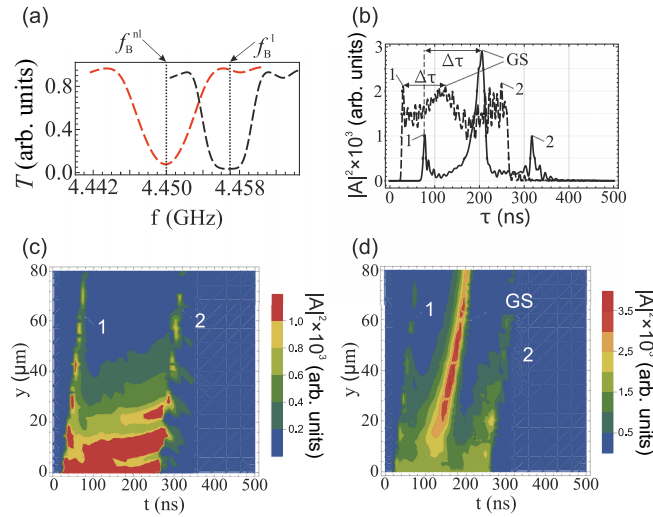


FIG. 9. (a) Transmission coefficient dependence on the frequency at input pulse amplitudes $A_0 = 0.03$ (black curve) and $A_0 = 0.04$ (red curve). (b) The envelope amplitude at the output of MC at the distances $l = 22 \mu\text{m}$ (dashed curve) and $l = 80 \mu\text{m}$ (solid curve) (the frequency corresponding, to the BG center, $H = 560 \text{ Oe}$, $\tau = 300 \text{ ns}$). Contour plots of evolution of the pulse envelope amplitude at (c) $A_0 = 0.03$ and (d) $A_0 = 0.04$. Label “1” is the splash corresponding to the leading edge, label “2” the splash corresponding to the trailing edge, and label “GS” is the gap soliton.

IV. NUMERICAL CALCULATION

Numerical solution of the equations was carried out under the following initial and boundary conditions: $A(y, 0) = B(y, 0) = B(l, t) = 0$, where A_0 is the amplitude of the input pulse; the function $f(t) = \begin{cases} A_0, & \text{at } \tau_0 - \tau/2 < t < \tau_0 + \tau/2 \\ 0, & \text{at } t > \tau_0 + \tau/2, t < \tau_0 - \tau/2 \end{cases}$ defines the rectangular shape of the input pulse; τ and τ_0 are the duration and delay of the input pulse, respectively; and l is the length of the structure.

Let us introduce the transmission coefficient of the MC in the following form: $T = \int_0^{t_{\max}} |A(l, t)|^2 dt / \int_0^{t_{\max}} |A(0, t)|^2 dt$, where t_{\max} is the observation time. Figure 9(a) shows the dependence of the transmission coefficient on the signal frequency for the linear case ($A_0 = 0.01$, black curve) and the nonlinear case ($A_0 = 0.04$, red curve). It can be seen that in each case the transmission coefficient has a pronounced minimum, which corresponds to the center of the band gap. The band gap is formed at $k_0 = k_{-1} = \pi/L$ and $\omega_B^2 = \frac{\omega_\perp^2 + \omega_M^2 d_0 k_0}{2\omega}$. In the linear case at small input signal amplitude, the center frequency of the BG is f_B^l . When the input amplitude increases, there is a nonlinear shift of the BG to the low-frequency region. The center frequency of the BG in this case is f_B^{nl} . Note that the effect of the nonlinear shift of the BG is theoretically described for spin waves in single and coupled MCs [15,37,47].

If the frequency of the input signal lies near the center frequency of the BG, we can assume $k_0 = k_{-1}$, and then $V_{0,-1} = V$, $\kappa_{0,-1} = \kappa$, $\gamma_{0,-1} = \gamma$, and $\eta_{0,-1} = \eta$. We choose the input signal frequency in the center of the BG in the linear case ($f = f_B^l$). In this case, in Eq. (4) we have $\eta = 0$ as the detuning of the signal frequency from the BG center frequency.

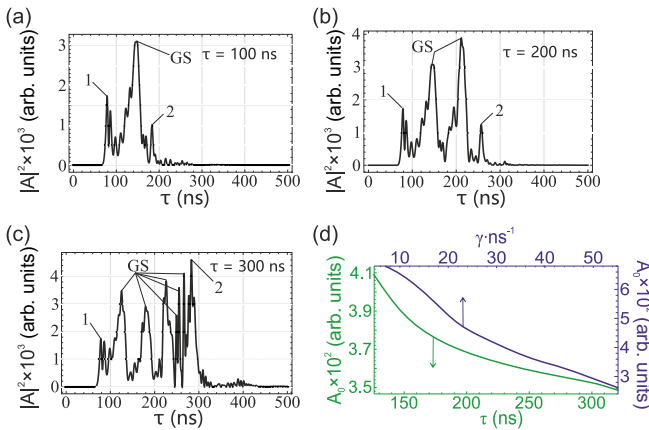


FIG. 10. The envelope amplitude at the output of MC ($l = 80 \mu\text{m}$) at $H_0 = 560 \text{ Oe}$ at the frequency corresponding to the BG center, input pulse amplitude $A_0 = 0.05$, and input pulse durations 100 ns (a), 200 ns (b), and 300 ns (c). (d) Dependence of the threshold amplitude for the GS formation on the duration of the input pulse (green curve). Dependence of the threshold amplitude for the GS formation on the parameter of nonlinearity γ (blue curve) ($H = 560 \text{ Oe}$, $\tau = 300 \text{ ns}$).

Let us consider the features of rectangular pulse propagation depending on the amplitude of the input signal according to the results of numerical calculation of Eq. (4). Figures 9(c) and 9(d) show the contour plots of evolution of the envelope amplitude at different input signal amplitudes. When the input signal amplitude is small, the pulse is almost completely reflected from the MC as a linear Bragg grating. Only two splashes with an interval equal to the input pulse duration can be observed in the output signal. These splashes correspond to the leading and trailing edge of the rectangular pulse [marked by the arrows 1 and 2 in Figs. 9(c) and 9(d)]. When the input amplitude exceeds the threshold amplitude, an additional pulse—a gap soliton—is formed in the output signal between the splashes [marked with an arrow, GS, in Fig. 9(d)]. Figure 9(b) shows the envelopes of the pulses at different distances from the input. It can be seen that the delay between the maximum of the GS and the leading edge splash $\Delta\tau$ increases along the propagation direction; i.e., the speed of the GS propagation is less than the group velocity in a homogeneous film (with which the leading and trailing edges of the input pulse propagate).

Figures 10(a)–10(c) show the amplitude of the output pulse envelope at different input pulse durations. Figure 10(a) shows that, at the input pulse duration of 100 ns, a single gap soliton is formed, which is consistent with the experimental data in Fig. 10(a). Figure 10(b) shows that, at the input pulse duration of 200 ns, two gap solitons are formed, which corresponds to the data in Fig. 6(d). Figure 10(c) shows that at the input pulse duration of 300 ns, six gap solitons are formed, which corresponds to the data in Fig. 7(a). It can be seen that increasing the input pulse duration increases the number of GSs. The threshold amplitude for GS formation decreases with the increasing input pulse duration, as shown by the green line in Fig. 10(d). With increasing the nonlinearity parameter γ , the threshold for the gap soliton formation decreases, as shown by the blue line in Fig. 10(d).

Thus, the developed theoretical model allows us to reveal the mechanism of gap soliton formation associated with the capture of spin-wave excitations on direct and reflected waves at the frequency of the band gap when the amplitude of the input signal increases. The model also describes the shift of the MC band gap due to nonlinear changes in the magnetization of the ferromagnetic medium, the increase in the number of gap solitons with increasing input signal amplitude, and the dependence of the gap soliton formation threshold on the input pulse duration, as observed in the experiment.

V. CONCLUSION

Thus, in summary, the main nonlinear features of spin waves propagating in a magnonic nanoscale magnonic crystal based on YIG film with a periodic system of grooves on the surface were investigated and described. The theoretical results were obtained using the coupled-waves method for direct wave and wave reflected from the spatial inhomogeneities of the periodic structure. The microwave method for measuring the frequency response and envelope amplitudes of propagating spin-wave pulses was applied. It was shown that the Bragg resonance condition is fulfilled in the spectrum of spin waves in the investigated structure and that the BG formation at the Bragg frequency and Bragg wave number takes place. When the input power increases from -8 to 10 dBm , there is a nonlinear shift of BG down the frequency by the order of 10 MHz . It was shown that at propagation of pulses of 50- to 300-ns duration in the investigated structure at frequencies inside the BG a special type of envelope soliton—gap solitons—can be formed. The formation of gap solitons was observed at increasing the input signal power in the range from -8 to 10 dBm . The threshold power for the formation of solitons decreased with increasing the input pulse duration. When increasing the duration and power of the input pulse, a series of GSs with a duration of about 10 ns was formed. It was found that the threshold power of the formation of GSs depends on the magnetic field magnitude. When pulses propagated at frequencies outside the BG, the pulse shape changed insignificantly.

A theoretical model describing the spatiotemporal evolution of the spin-wave pulse envelope in the investigated structure was constructed. This model allows us to reveal the mechanism of the GS formation due to the capture of spin-wave excitations of the direct and reflected waves at the frequency inside the BG when the amplitude of the input signal increases. The velocity of the GS is smaller than the group velocity of a spin wave in a homogeneous film and the velocity of a linear pulse in an MC and increases with increasing amplitude.

The results obtained in this work allow us to consider nanoscale periodic YIG structures as promising candidates for frequency-selective devices for information transmission and encoding using gap solitons.

ACKNOWLEDGMENT

The work was supported by the Russian Science Foundation (Project No. 23-79-30027).

- [1] A. Mahmoud, F. Ciubotaru, F. Vanderveken, A. V. Chumak, S. Hamdioui, C. Adelman, and S. Cotozana, Introduction to spin wave computing, *J. Appl. Phys.* **128**, 161101 (2020).
- [2] A. Barman, G. Gubbiotti, S. Ladak, A. O. Adeyeye, M. Krawczyk *et al.*, The 2021 magnonics roadmap, *J. Phys.: Condens. Matter* **33**, 413001 (2021).
- [3] A. V. Chumak, P. Kabos, M. Wu, C. Abert, C. Adelman *et al.*, Advances in magnetics roadmap on spin-wave computing, *IEEE Trans. Magn.* **58**, 0800172 (2022).
- [4] Q. Wang, A. V. Chumak, L. Jin, H. Zhang, B. Hillebrands, and Z. Zhong, Voltage-controlled nanoscale reconfigurable magnonic crystal, *Phys. Rev. B* **95**, 134433 (2017).
- [5] H. Merbouche, I. Boverter, V. Haspot, S. Fusil, V. Garcia, D. Gouéré, C. Carrétéro, A. Vecchiola, R. Lebrun, P. Bortolotti, L. Vila, M. Bibes, A. Barthélémy, and A. Anane, Voltage-controlled reconfigurable magnonic crystal at the sub-micrometer scale, *ACS Nano* **15**, 9775 (2021).
- [6] A. Roxburgh and E. Iacocca, Nano-magnonic crystals by periodic modulation of magnetic parameters, *Magnetochemistry* **10**, 14 (2024).
- [7] V. V. Kruglyak, S. O. Demokritov, and D. Grundler, Magnonics, *J. Phys. D* **43**, 260301 (2010).
- [8] A. A. Serga, A. V. Chumak, and B. Hillebrands, Yig magnonics, *J. Phys. D* **43**, 264002 (2010).
- [9] Q. Wang, B. Heinz, R. Verba, M. Kewenig, P. Pirro, M. Schneider, T. Meyer, B. Lägel, C. Dubs, T. Brächer, and A. V. Chumak, Spin pinning and spin-wave dispersion in nanoscopic ferromagnetic waveguides, *Phys. Rev. Lett.* **122**, 247202 (2019).
- [10] J. Adam, L. Davis, G. Dionne, E. Schloemann, and S. Stitzer, Ferrite devices and materials, *IEEE Trans. Microwave Theory Tech.* **50**, 721 (2002).
- [11] C. Dubs, O. Surzhenko, R. Thomas, J. Osten, T. Schneider, K. Lenz, J. Grenzer, R. Hübner, and E. Wendler, Low damping and microstructural perfection of sub-40nm-thin yttrium iron garnet films grown by liquid phase epitaxy, *Phys. Rev. Mater.* **4**, 024416 (2020).
- [12] G. Schmidt, C. Hauser, P. Trempler, M. Paleschke, and E. T. Papaioannou, Ultra thin films of yttrium iron garnet with very low damping: A review, *Phys. Status Solidi (b)* **257**, 1900644 (2020).
- [13] M. Krawczyk and D. Grundler, Review and prospects of magnonic crystals and devices with reprogrammable band structure, *J. Phys.: Condens. Matter* **26**, 123202 (2014).
- [14] A. V. Chumak, A. A. Serga, B. Hillebrands, and M. P. Kostylev, Scattering of backward spin waves in a one-dimensional magnonic crystal, *Appl. Phys. Lett.* **93**, 022508 (2008).
- [15] A. B. Ustinov, A. V. Drozdovskii, and B. A. Kalinikos, Multifunctional nonlinear magnonic devices for microwave signal processing, *Appl. Phys. Lett.* **96**, 142513 (2010).
- [16] P. Frey, A. A. Nikitin, D. A. Bozhko, S. A. Bunyaev, G. N. Kakazei, A. B. Ustinov, B. A. Kalinikos, F. Ciubotaru, A. V. Chumak, Q. Wang, V. S. Tiberkevich, B. Hillebrands, and A. A. Serga, Reflection-less width-modulated magnonic crystal, *Commun. Phys.* **3**, 17 (2020).
- [17] M. Morozova, D. Romanenko, A. Serdobintsev, O. Matveev, Y. Sharaevskii, and S. Nikitov, Magnonic crystal-semiconductor heterostructure: Double electric and magnetic fields control of spin waves properties, *J. Magn. Magn. Mater.* **514**, 167202 (2020).
- [18] A. B. Ustinov, A. V. Drozdovskii, A. A. Nikitin, A. A. Semenov, D. A. Bozhko, A. A. Serga, B. Hillebrands, E. Lähderanta, and B. A. Kalinikos, Dynamic electro-magnonic crystal based on artificial multiferroic heterostructure, *Commun. Phys.* **2**, 137 (2019).
- [19] M. A. Morozova, S. V. Grishin, A. V. Sadovnikov, D. V. Romanenko, Y. P. Sharaevskii, and S. A. Nikitov, Tunable bandgaps in layered structure magnonic crystal–ferroelectric, *IEEE Trans. Magn.* **51**, 2802504 (2015).
- [20] S. E. Sheshukova, E. N. Beginin, A. V. Sadovnikov, Y. P. Sharaevskii, and S. A. Nikitov, Multimode propagation of magnetostatic waves in a width-modulated yttrium-iron-garnet waveguide, *IEEE Magn. Lett.* **5**, 3700204 (2014).
- [21] A. A. Nikitin, A. B. Ustinov, A. A. Semenov, A. V. Chumak, A. A. Serga, V. I. Vasyuchka, E. Lähderanta, B. A. Kalinikos, and B. Hillebrands, A spin-wave logic gate based on a width-modulated dynamic magnonic crystal, *Appl. Phys. Lett.* **106**, 102405 (2015).
- [22] Y. V. Khivintsev, Y. A. Filimonov, and S. Nikitov, Spin wave excitation in yttrium iron garnet films with micron-sized antennas, *Appl. Phys. Lett.* **106**, 052407 (2015).
- [23] H. Qin, G.-J. Both, S. J. Hämäläinen, L. Yao, and S. van Dijken, Low-loss YIG-based magnonic crystals with large tunable bandgaps, *Nat. Commun.* **9**, 5445 (2018).
- [24] M. A. Morozova, O. V. Matveev, A. M. Markeev, A. G. Chernikova, A. M. Mednikov, S. A. Gusev, I. Y. Pashenkin, N. S. Gusev, D. V. Romanenko, and S. A. Nikitov, Magneto-electric hysteresis of bragg resonances in a multiferroic crystal based on YIG/HZO, *Phys. Rev. B* **108**, 174407 (2023).
- [25] P. E. Wigen, Nonlinear phenomena and chaos in magnetic materials, in *Nonlinear Phenomena and Chaos in Magnetic Materials* (World Scientific, Singapore, 1994), pp. 1–12.
- [26] A. Zvezdin and A. Popkov, Contribution to the nonlinear theory of magnetostatic spin waves, *Zh. Eksp. Teor. Fiz.* **84**, 606 (1983) [*Sov. Phys. JETP* **57**, 350 (1983)].
- [27] G. C. Ádám Papp and W. Porod, Nanoscale neural network using non-linear spin-wave interference, *Nat. Commun.* **12**, 6422 (2021).
- [28] G. Tanaka, T. Yamane, J. B. Héroux, R. Nakane, N. Kanazawa, S. Takeda, H. Numata, D. Nakano, and A. Hirose, Recent advances in physical reservoir computing: A review, *Neural Networks* **115**, 100 (2019).
- [29] S. Watt and M. Kostylev, Reservoir computing using a spin-wave delay-line active-ring resonator based on yttrium-iron-garnet film, *Phys. Rev. Appl.* **13**, 034057 (2020).
- [30] S. V. Grishin, Y. P. Sharaevskii, S. A. Nikitov, E. N. Beginin, and S. E. Sheshukova, Self-generation of chaotic dissipative soliton trains in active ring resonator with 1-D magnonic crystal, *IEEE Trans. Magn.* **47**, 3716 (2011).
- [31] N.-N. Chen, A. N. Slavin, and M. G. Cottam, Gap solitons in periodic structures: Modulated magnetic thin films, *Phys. Rev. B* **47**, 8667 (1993).
- [32] Q. Wang, J.-l. Shi, and J.-s. Bao, Theory of nonlinear magnetostatic surface wave in a periodically corrugated ferromagnetic slab, *J. Appl. Phys.* **77**, 5831 (1995).
- [33] A. B. Ustinov, B. A. Kalinikos, V. E. Demidov, and S. O. Demokritov, Formation of gap solitons in ferromagnetic films with a periodic metal grating, *Phys. Rev. B* **81**, 180406(R) (2010).

- [34] N. Kumar, P. Gruszecki, M. Gołbiewski, J. W. Klos, and M. Krawczyk, Exciting high-frequency short-wavelength spin waves using high harmonics of a magnonic cavity mode, *Adv. Quantum Technol.* **7**, 2400015 (2024).
- [35] M. M. Scott, C. E. Patton, M. P. Kostylev, and B. A. Kalinikos, Nonlinear damping of high-power magnetostatic waves in yttrium–iron–garnet films, *J. Appl. Phys.* **95**, 6294 (2004).
- [36] U.-H. Hansen, V. E. Demidov, and S. O. Demokritov, Dual-function phase shifter for spin-wave logic applications, *Appl. Phys. Lett.* **94**, 252502 (2009).
- [37] S. Sheshukova, M. Morozova, E. Beginin, Y. P. Sharaevskii, and S. Nikitov, Formation of gap solitons in a finite magnonic crystal, *Phys. Wave Phenom.* **21**, 304 (2013).
- [38] B. A. Malomed, *Soliton Management in Periodic Systems* (Springer, Berlin, 2006).
- [39] B. Kalinikos and A. Slavin, Theory of dipole-exchange spin wave spectrum for ferromagnetic films with mixed exchange boundary conditions, *J. Phys. C* **19**, 7013 (1986).
- [40] H. Qin, S. J. Hämäläinen, K. Arjas, J. Witteveen, and S. van Dijken, Propagating spin waves in nanometer-thick yttrium iron garnet films: Dependence on wave vector, magnetic field strength, and angle, *Phys. Rev. B* **98**, 224422 (2018).
- [41] M. Morozova, O. Matveev, D. Romanenko, Y. P. Sharaevsky, and S. Nikitov, Gap solitons in heterostructure magnonic crystal/semiconductor, *J. Phys. D* **55**, 385001 (2022).
- [42] S. Baskakov, *Signals and Circuits* (Mir, Moscow, 1986), p. 520.
- [43] Y. S. Kivshar and G. P. Agrawal, *Optical Solitons: From Fibers to Photonic Crystals* (Academic, San Diego, 2003).
- [44] D. Stancil and A. Prabhakar, *Spin Waves: Theory and Applications* (Springer US, New York, 2009).
- [45] L. Brillouin, *Wave Propagation in Periodic Structures* (Dover, New York, 1946).
- [46] D. Marcuse, *Theory of Dielectric Optical Waveguides* (Elsevier, Amsterdam, 2013).
- [47] M. Morozova, O. Matveev, D. Romanenko, A. Trukhanov, A. Mednikov, Y. P. Sharaevskii, and S. Nikitov, Nonlinear spin wave switches in layered structure based on magnonic crystals, *J. Magn. Magn. Mater.* **508**, 166836 (2020).